DOI: 10.13009/EUCASS2019-269

DOI: ADD DOINUMBER HERE

A Sliding Mode Control in a Backstepping Setup for Rendezvous Mission on a Circular Orbit

Zenteno Torres Jazmín [†], *Cieslak Jérôme*[†], *Henry David*[†,‡], *Dávila Jorge*[⋆]
[†]: *IMS lab., Univ. Bordeaux, Bordeaux INP, CNRS (UMR 5218), 351 cours de la libération, 33405 Talence, France*
{jazmin.zenteno-torres,jerome.cieslak,david.henry}@ims-bordeaux.fr
[⋆]: Instituto Politécnico Nacional IPN, Av. Ticoman 600, Mexico D.F. (jadavila@ipn.mx)
[‡]Corresponding author

Abstract

The general context of this paper is the assessment of Sliding Mode Control (SMC) techniques for rendezvous missions in space, under realistic simulations, i.e. considering the coupling between attitude and translational motions, propellant sloshing, flexible modes of the solar arrays and the most dimensioning space disturbances (i.e. second zonal harmonic J_2, atmospheric drag, magnetic disturbance, gravity gradient and solar radiation pressure). A SMC technique fitted with a state feedback linearisation is proposed in a backstepping setup. Simulation results demonstrate the potential of the proposed solution.

1. Introduction

In missions of spacecraft interceptions or in-orbit assembly tasks, there is a need to provide Guidance Navigation and Control (GNC) solutions to accurately and automatically achieve the rendezvous and the capture phases, in an uncertain and disturbed environment. The work addressed in this paper must be understood in this context. The aim is to assess the potential of Sliding Mode Control (SMC) techniques for autonomous rendezvous in space on a circular orbit with a passive target, i.e. the target has no sensor, no actuator and no onboard telemetry data processing algorithm so that it cannot neither communicate with the ground stations, nor with the chaser spacecraft that is in charge of capture.

In such a context, the design of robust controllers for automatic rendezvous is a topic of great importance. In the literature, several control theories have been used to tackle such a problem, e.g. by using H_∞ theory (Gao et al., 2012), gain scheduling concept (Wang et al., 2015) and adaptive control strategies (Zhao et al., 2013) to name a few. Note that the recent non-smooth H_∞ theory is currently investigated by the European Space Agency (ESA) through numerous research projects, like microvibrations mitigation for satellite observation mission that requires high pointing stability (Preda et al., 2017, 2018), autonomous assembly in space of huge flexible structures like telescopes (Colmenarejo et al., 2018b) or autonomous debris removal like the e.Deorbit mission that aims at removing the defunct Envisat satellite from the Earth orbit (Colmenarejo et al., 2017, 2018a; Henry et al., 2019).

Another control technique that receives recently attention in the research community is the backstepping technique. Backstepping is an iterative approach that uses part of the states as virtual controls to drive the other states. It has, as one disadvantage, performance degradation under the presence of parametric uncertainties. Solutions have been proposed in literature adding to the backstepping approach other control techniques, see for example backstepping with a PID in (Krogstad et al., 2007), optimal control in (Krstic and Tsiotras, 1999) or sliding-mode control (SMC) techniques (De Loza et al., 2015; Zenteno-Torres et al., 2019). In this paper, the focus is on this latest technique.

SMC theory has received a growing attention during the two last decades, mainly due to the famous finite-time and insensitivity properties against matched perturbations (i.e. those which impact directly the input channels, see (Shtessel et al., 2014)). Within the aerospace area, the SMC technique has been firstly applied for attitude stabilization in the 90's, see (Lo and Chen, 1995) and (Crassidis and Markley, 1996). In (Park et al., 1999), a two-step SMC scheme is proposed to tackle the earth's gravitational disturbance. A SMC strategy has been developed for an exoatmospheric interceptor in (Ebrahimi et al., 2008). In (Imani and Beigzadeh, 2016), two controllers are designed using optimal sliding-mode control and backstepping for attitude control of a spacecraft in elliptical orbit considering the J_2 and atmospheric drag disturbances. The approach is based on a SMC law fitted by an integral. A solution for automatic space

DOI: 10.13009/EUCASS2019-269

rendezvous and docking is proposed in (Tournes et al., 2011) using a second order sliding mode control approach. In (Liu et al., 2016), the authors propose a SMC solution for rendezvous and docking with a tumbling spacecraft based on the backstepping technique. In (Cong et al., 2013), a backstepping based adaptive sliding-mode control is used for the attitude control of a spacecraft with uncertainties. Recently, the works reported in (Huang and Jia, 2017) and (Dong et al., 2017) propose an alternative approach by using an adaptive mechanism, for spacecraft rendezvous. An attitude controller for a spacecraft is designed (Davila and Gómez-Cortes, 2013) using backstepping techniques based on High Order Sliding-Modes (HOSM).

Even if these results are promising, they do not consider the solar arrays and propellant sloshing effects which creates a coupling between rotational and translational dynamics. Although in (Hu et al., 2009) solar arrays are considered, the designed controller is dedicated for the spacecraft's attitude. The contribution of the paper must be thought in this context. Controllers for attitude and translational dynamics are designed based on SMC combined with backstepping, given that the coupling effect appears when considering propellant sloshing effects, flexible modes of the solar arrays and the most dimensioning space disturbances, i.e. second zonal harmonic J_2, atmospheric drag, magnetic disturbance, gravity gradient and solar radiation pressure. Attitude and position control is considered in (Zenteno-Torres et al., 2018, 2019), but is limited to the influence of the flexible modes of the solar arrays, i.e. propellant sloshing is not considered.

The paper is organized as follows. Section 2 briefly recalls the theory of the proposed SMC algorithm. Section 3 is devoted to the space mission and presents the results.

2. Material backgrounds

In the interest of brevity, throughout this section an earnest attempt will be made to avoid duplicating material presented in (Zenteno-Torres et al., 2018). Towards this end, the focus of this section will lie wholly with the results summarized by theorem 1. Thus, we will assume the reader is familiar with the developments presented in (Zenteno-Torres et al., 2018), and will often refer the reader to this paper for necessary backgrounds and proofs.

Consider the following form of a system's model, composed into two connected sub-systems

$$\begin{aligned}\begin{bmatrix}\dot{x}_1\\ \dot{x}_2\end{bmatrix} &= \begin{bmatrix}A_{11} & A_{12}\\ A_{21} & A_{22}\end{bmatrix}\begin{bmatrix}x_1\\ x_2\end{bmatrix} + \begin{bmatrix}0\\ I_m\end{bmatrix}(u+v)\\ \begin{bmatrix}y\\ x_2\end{bmatrix} &= \begin{bmatrix}C_1 & 0\\ 0 & \mathbb{I}_m\end{bmatrix}\begin{bmatrix}x_1\\ x_2\end{bmatrix}\end{aligned} \tag{1}$$

Here $x = [x_1^T \; x_2^T]^T \in \mathbb{R}^n$, $u \in \mathbb{R}^m$ and $v \in \mathbb{R}^m$ refer to the system's state, control input and (matched) disturbance vectors respectively. The sub-system defined by the first state equation represents the sub-actuated dynamics and the second state equation corresponds to the actuated dynamics. Thus, $x_1 \in \mathbb{R}^{n-m}$ and $x_2 \in \mathbb{R}^m$. The matrices $A_{ij}, i, j = 1, 2$ and C_1 are of adequate dimension.
The goal we pursue is to design the state feedback sliding mode control law that obeys to a backstepping paradigm so that $y(t)$ follows an *a priori* given trajectory $y_c(t)$, $\forall t \geq 0$.

The following assumptions are made:

A.1) The component v_j of v are bounded, i.e. $|v_j| \leq v_j^+$ and thus $\|v\|_\infty \leq \infty$.

A.2) The time derivatives of $y_c(t)$ up to order 2 are assumed to be available.

Assumption A.1 is a well known condition for the existence of a first generation sliding mode control, see (Shtessel et al., 2014) for instance. Assumption A.2 is reasonable from a practical point of view since the time derivatives of $y_c(t)$ are generally endogenous signals in a trajectory planing algorithm. Sliding mode-based differentiation techniques can be used in case of, see (Levant, 2003; Mboup et al., 2007). Analysis of these techniques is out of the scope of the paper.

Remark 1 *It can be noted from equation* (1) *that x_2 is assumed to be measured. This assumption can obviously be relaxed by using a state estimator. There exist multiple techniques to address this issue. Within the sliding mode setting, one can mention the HOSM observer approach, see for instance (De Loza, Cieslak, Henry, Zolghadri, and Fridman, 2015). Designing such an estimator is out of the scope of this paper, so it is not addressed in the following.*

DOI: 10.13009/EUCASS2019-269

The backstepping strategy proposed in (Zenteno-Torres et al., 2018) can be sum up as follows:

Define the tracking error $e_y = y_c - y$ and the following control law u:

$$u = \dot{\phi} - A_{21}x_1 - A_{22}x_2 - \alpha sign(e_\phi) + (C_1A_{12})^T e_y - L_2 e_\phi \tag{2}$$

This first order sliding-mode control law consists of two parts, a linear part (say u_0) and a discontinuous part (say u_d) so that $u = u_0 + u_d$, where u_0 corresponds to the feedback linearization by backstepping approach and u_d corresponds to the sliding-mode term used to compensate the disturbances. In this equation:

- the sliding gain matrix α is defined according to $\alpha = diag(\alpha_j)$ with $\alpha_j > 0 \forall j$;
- ϕ and the error e_ϕ are defined according

$$\phi = (C_1A_{12})^+(\dot{y}_c - C_1A_{11}x_1 + L_1e_y) \tag{3}$$

$$e_\phi = \phi - x_2 \tag{4}$$

- $L_1 \in \mathbb{R}^{m\times m}$ and $L_2 \in \mathbb{R}^{m\times m}$ are matrices to be designed.

The following theorem gives the solution to the control design problem:

Theorem 1 *Consider the system* (1) *with the SMC law* (2)*. The closed loop is asymptotically stable and the controller* (2) *tracks the reference signal* y_c *while annihilating* v *(matched perturbations) if (sufficient condition)* $L_k < 0, k = 1, 2$ *and* $\alpha_j > v_j^+, \forall j$.

Proof: see (Zenteno-Torres et al., 2018).

Tuning $L_k, k = 1, 2$ enables to manage the convergence time of $x_2(t)$ to $\phi(t)$ and $x_1(t)$ to $x_{1c}(t)$, so it is for $y(t)$ to $y_c(t)$. Therefore, the convergence time of $e_\phi(t)$ to zero can be reduced if L_1 has small eigenvalues (fast dynamics). Similarly, the eigenvalues of L_2 enables to manage the closed loop dynamics, see equation (2).

3. Application to a rendezvous mission

3.1 The reference scenario

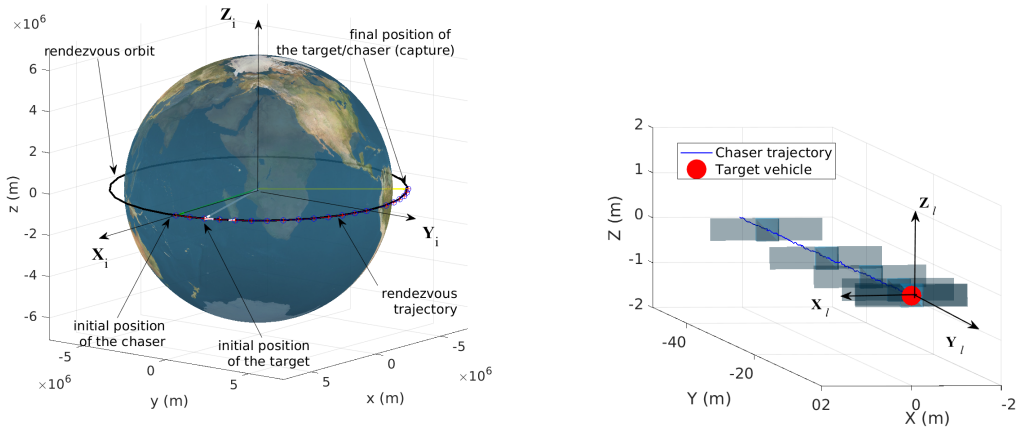

Figure 1: The orbit and rendezvous trajectory in $\mathcal{F}_i$ (left) and in the LVLH frame $\mathcal{F}_l$ (right). The trajectory corresponds to the results in section 3.4

The reference scenario consists of two vehicles inserted into the same circular orbit around Earth. One vehicle (the target) is a passive spacecraft (i.e. no sensors and actuators) while the second one (the chaser), is equipped by a set of rendezvous sensors and actuators and a complete GNC (Guidance and Navigation Control) unit. The characteristics of the orbit's rendezvous are a semi-major axis $a = 7068$ km, an eccentricity $e = 0$ and an inclination $i = 0$ deg.

DOI: 10.13009/EUCASS2019-269

The trajectories of the spacecraft on this orbit are characterized by constant longitude of the ascending node and argument of periapsis (fixed to $\Omega = 0rad$ and $\omega = 0rad$ respectively) with initial values of the true anomaly fixed to $\nu(0) = 1,5.10^{-5}rad$ for the target and $\nu(0) = 0rad$ for the chaser. With these orbital parameters, the initial distance between the two spacecraft is $100m$ approximatively in the $-y$-axis direction in the so called Local Vertical Local Horizontal (LVLH) frame $\mathcal{F}_l = \{O_t; \overrightarrow{\mathbf{X_l}}, \overrightarrow{\mathbf{Y_l}}, \overrightarrow{\mathbf{Z_l}}\}$[1]. The spacecraft trajectories in the inertial frame $\mathcal{F}_i = \{O_E; \overrightarrow{\mathbf{X_i}}, \overrightarrow{\mathbf{Y_i}}, \overrightarrow{\mathbf{Z_i}}\}$[2] and in $\mathcal{F}_l$ are illustrated on Fig. 1 for a better understanding. The considered rendezvous trajectory corresponds to *i*) target acquisition where the chaser keeps its position at its initial position and rotates to acquire the target and *ii*) rendezvous where the chaser's attitude is controlled to keep the capture mechanism aligned with the target and while, at the same time, it performs a forced translation.

The avionics architecture retained for the mission, is composed of a LIDAR which provides relative positions and velocities, an IMU and a Star Tracker. It is worth noting that, in this work, it is assumed a perfect navigation unit, i.e. all the measurements are assumed to be noise free. The actuation consists of 12 thrusters of $4N$ for both attitude and position control.

The complete mission is modelled into a so-called functional engineering simulator developed in Matlab/Simulink. Both chaser and target have each one an associated environment module as some characteristics depend on specific spacecraft properties. Typically, the chaser has two half-filled tanks that cause propellant sloshing and a solar array with two flexible modes, whereas the target is assumed to be a spherical object. For the chaser, the considered disturbances are the second-order zonal harmonic J_2, the atmospheric drag, the gravity gradient and effect of the Earth magnetic filed. With regard to the target, it is assumed to be affected by the J_2 disturbance and the atmospheric drag.

3.2 Modelling issues

In the following, we use the notations $\mathsf{v}^i, \mathsf{v}^l, \mathsf{v}^b$ to refer to a variable v given in the frame $\mathcal{F}_i, \mathcal{F}_l, \mathcal{F}_b$, respectively. $\mathcal{F}_b = \{O_b; \overrightarrow{\mathbf{X_b}}, \overrightarrow{\mathbf{Y_b}}, \overrightarrow{\mathbf{Z_b}}\}$ is the chaser's body frame.[3] The superscript "i", "l", "b" is omitted when there exists no ambiguity.

3.2.1 Modelling the relative translational motion between the two spacecraft

Let (x_c, y_c, z_c) be the coordinates of the chaser's center of mass (CoM), in $\mathcal{F}_i$. Then, the dynamics of the chaser's translational motion is described according to (Wied, 1998; Montenbruck and Gill, 2012):

$$\dot{\mathbf{x}}_c^i = f(\mathbf{x}_c^i) + \begin{bmatrix} 0_3 \\ \mathbb{I}_3 \end{bmatrix} (\gamma_u^i + \gamma_{sl}^i + \gamma_{sa}^i + \gamma_{dc}^i) \tag{5}$$

In this equation $\mathbf{x}_c^i = [x_c\, y_c\, z_c\, \dot{x}_c\, \dot{y}_c\, \dot{z}_c]^T$ is the state vector composed by the position and velocities of the chaser along each axis of $\mathcal{F}_i$ and $\gamma_u^i, \gamma_{sl}^i, \gamma_{sa}^i, \gamma_{dc}^i$ refer to the 3-dimensional accelerations due to the propulsion unit, propellant sloshing, flexible appendages and disturbances respectively.
Similarly, let (x_t, y_t, z_t) be the coordinates of the target's CoM in $\mathcal{F}_i$. Then, the dynamics of the target's translational motion can be described according to

$$\dot{\mathbf{x}}_t^i = f(\mathbf{x}_t^i) + \begin{bmatrix} 0_3 \\ \mathbb{I}_3 \end{bmatrix} \gamma_{dt}^i \tag{6}$$

where $\mathbf{x}_t^i = [x_t\, y_t\, z_t\, \dot{x}_t\, \dot{y}_t\, \dot{z}_t]^T$ is the state vector composed by the positions and velocities of the target. γ_{dt}^i refers to the disturbances (accelerations) about the target's CoM.

[1] The origin of the LVLH frame is at the target center of mass, the axis $\overrightarrow{\mathbf{Z_l}}$ is pointing to the opposite of O_E, the axis $\overrightarrow{\mathbf{Y_l}}$ is aligned with the negative orbital momentum vector and $\overrightarrow{\mathbf{X_l}}$ completes the frame.

[2] The inertial frame $\mathcal{F}_i$ is defined as on Fig. 1

[3] The center of this frame coincides with the chaser's CoM and its axes are oriented in such a way that an attitude angle equal to $[0\,0\,0]^T$ means that the chaser is aligned with the target.

DOI: 10.13009/EUCASS2019-269

In Eq. (5) and (6), the nonlinear state dependent function $f(\mathbf{x}_j^i)$, $j \in \{c,t\}$ is given by

$$f(\mathbf{x}_j^i) = \begin{bmatrix} \dot{x}_j \\ \dot{y}_j \\ \dot{z}_j \\ \frac{-\mu x_j}{\left(x_j^2+y_j^2+z_j^2\right)^{3/2}} \\ \frac{-\mu y_j}{\left(x_j^2+y_j^2+z_j^2\right)^{3/2}} \\ \frac{-\mu z_j}{\left(x_j^2+y_j^2+z_j^2\right)^{3/2}} \end{bmatrix} \; j \in \{c,t\} \tag{7}$$

$\mu = Gm_E$ is the Earth gravitational constant where G and m_E are the universal gravitational constant and the mass of the Earth planet, respectively.

Subscribing Eq. (6) to Eq. (5) leads to the relative translational motion between the two spacecraft, given in $\mathcal{F}_i$. The result is a state space model that involves the relative position $\Delta x^i = x_c^i - x_t^i$ and the relative velocities $\Delta \dot{x}^i = \dot{x}_c^i - \dot{x}_t^i$.

Now, consider the rotation matrix $\mathcal{R}_i^l(a,e,i,\Omega,\omega,\nu)$ that performs the projection of a vector $\mathbf{v} \in \mathbb{R}^3$ from $\mathcal{F}_i$ to $\mathcal{F}_l$, see (Montenbruck and Gill, 2012). With the retained target orbital parameters (see section 3.1), it can be verified that $\mathcal{R}_i^l(a,e,i,\Omega,\omega,\nu)$ depends only on the semi-major axis a and the true anomaly ν, that is $\mathcal{R}_i^l(a,\nu)$. Applying the change of coordinates $\rho = \mathcal{R}_i^l(a,\nu)\Delta x^i = [\eta\ \zeta\ \xi]^T$ (and therefore $\dot{\rho} = \mathcal{R}_i^l(a,\nu)\Delta \dot{x}^i = [\dot{\eta}\ \dot{\zeta}\ \dot{\xi}]^T$), it follows that the state space model that describes the dynamics of the relative translational motion between the two spacecrafts in $\mathcal{F}_l$, takes the form of (8) where $j = \{c,t\}$ and $g(.)$ is a function that depend nonlinearly on $\rho, \dot{\rho}, a, \nu, \gamma_{dj}^i$.

$$\begin{bmatrix} \dot{\rho} \\ \ddot{\rho} \end{bmatrix} = g(\rho,\dot{\rho},a,\nu,\gamma_{dj}^i) + \begin{bmatrix} 0_3 \\ \mathbb{I}_3 \end{bmatrix} \left(\frac{1}{m} F_u^l + \gamma_{sl}^l + \gamma_{sa}^l \right) \tag{8}$$

In Eq. (8), m is the total mass of the chaser's spacecraft, $F_u^l = m\mathcal{R}_i^l(a,\nu)\gamma_u^i$ is the three-dimensional forces due to the thruster-based propulsion unit, $\gamma_{sl}^l = m\mathcal{R}_i^l(a,\nu)\gamma_{sl}^i$ and $\gamma_{sa}^l = m\mathcal{R}_i^l(a,\nu)\gamma_{sa}^i$ are forces due to propellant sloshing and the flexible appendages respectively, given in $\mathcal{F}_l$.

Since the target follows a circular Keplerian orbit, the velocity of the true anomaly satisfies the third Kepler law, i.e.

$$\dot{\nu}^2 a^3 = \text{constant} = \mu = Gm_E \Rightarrow \dot{\nu} = \sqrt{\frac{\mu}{a^3}} = n \tag{9}$$

where $\mu = 3.9858 \times 10^{14}$. Then, because the distance between the target and the chaser during the rendezvous is much smaller than the orbit, i.e., $\|\rho\|_2 \ll a$, it is possible to perform a first order Taylor approximation of (8). This leads to the so called Clohessy-Wiltshire equations, also named the Hill equations (Wied, 1998; Montenbruck and Gill, 2012):

$$\begin{bmatrix} \dot{\rho} \\ \ddot{\rho} \end{bmatrix} = \begin{bmatrix} 0 & 0 & 0 & 1 & 0 & 0 \\ 0 & 0 & 0 & 0 & 1 & 0 \\ 0 & 0 & 0 & 0 & 0 & 1 \\ 3n^2 & 0 & 0 & 0 & 2n & 0 \\ 0 & 0 & 0 & -2n & 0 & 0 \\ 0 & 0 & -n^2 & 0 & 0 & 0 \end{bmatrix} \begin{bmatrix} \rho \\ \dot{\rho} \end{bmatrix} + \begin{bmatrix} 0_3 \\ \mathbb{I}_3 \end{bmatrix} \left(\tfrac{1}{m} F_u^l + \gamma_v^l\right) \tag{10}$$

In this equation, γ_v^l is a generalized disturbance acceleration which is an additive approximation of the effects that $\gamma_{sl}^l, \gamma_{sa}^l$ and $\gamma_{dj}^l = \mathcal{R}_i^l(a,\nu)\gamma_{dj}^i$, $j = \{c,t\}$ have on the dynamics of the relative position and relative velocity.

Remark 2 *It should be outlined that $\gamma_{sl}^l, \gamma_{sa}^l$ and γ_{dj}^i, $j = \{c,t\}$ enter endogenously the state space model* (8)*. So, approximating them into a form of a generalized exogenous signal γ_v^l must be validated. Especially such an approximation is valid if $\gamma_{sl}^l, \gamma_{sa}^l$ and γ_{dj}^i, $j = \{c,t\}$ do not destabilize the control loop that we will develop later. Fortunately, this has been revealed to be the case, see the simulation results presented in 3.4 that are obtained from the functional engineering simulator that does not consider any kind of approximation.*

3.2.2 Modelling the attitude of the chaser's spacecraft

The rotational motion of the chaser caused by an applied moment (sum of all torques acting on it) can be derived from the Euler's second law in the body frame $\mathcal{F}_b$ according to:

$$\dot{\varpi} = J^{-1} \sum_k T_k - J^{-1} \varpi \times J\varpi \tag{11}$$

DOI: 10.13009/EUCASS2019-269

Here, $\varpi = [p\ q\ r]^T$ is the angular velocity vector and $J \in \mathbb{R}^{3\times3}$ is the inertia matrix of the chaser's spacecraft without considering the solar array. In (11), $\sum_k T_k = T_u + T_{sl} + T_{sa} + T_d$ describes the sum of torques about the chaser's CoM, in $\mathcal{F}_b$. T_u refers to the moment caused by the thruster-based propulsion unit and T_{sl}, T_{sa}, T_d refer to the moment caused by propellant sloshing, the solar array and the exogenous disturbances.

Using the individual rotation matrices from Euler (3,2,1) rotation, the relationship between the rotational velocities ϖ and the rate of the Euler angles $\Theta = [\phi\ \theta\ \psi]^T$ is given after by

$$\dot{\Theta} = \frac{1}{\cos(\theta)} \begin{bmatrix} \cos(\theta) & \sin(\phi)\sin(\theta) & \cos(\phi)\sin(\theta) \\ 0 & \cos(\phi)\cos(\theta) & -\sin(\phi)\cos(\theta) \\ 0 & \sin(\phi) & \cos(\phi) \end{bmatrix} \varpi \tag{12}$$

Performing a first order Taylor approximation of Eqs. (11) and (12) around $\varpi = 0$ and $\Theta = 0$, leads to the following linear state space model of the attitude of the chaser:

$$\begin{bmatrix} \dot{\Theta} \\ \dot{\varpi} \end{bmatrix} = \begin{bmatrix} 0_3 & \mathbb{I}_3 \\ 0_3 & 0_3 \end{bmatrix} \begin{bmatrix} \Theta \\ \varpi \end{bmatrix} + \begin{bmatrix} 0_3 \\ J^{-1} \end{bmatrix} (T_u + T_v^b) \tag{13}$$

Here, T_v^b is a generalized disturbance moment (given in $\mathcal{F}_b$) which is an additive approximation of the effects that T_{sl}, T_{sa}, T_d have on the dynamics of the attitude and angular velocity. Note that since T_{sl}, T_{sa} are endogenous signals, a similar remark than remark 3 yields.

3.3 Derivation of the control law parameters

Coming back to equations (10) and (13), it is easy to see that if we define the control inputs and matched disturbances according to

- $u = \frac{1}{m} F_u^l$ and $v = \gamma_v^l$ in the case of (10). This is equivalent to say that the control signal is defined in terms of linear accelerations in the frame $\mathcal{F}_l$.
- $u = J^{-1} T_u$ and $v = J^{-1} T_v^b$ in the case of (13). This means that the control signal is defined in terms of angular accelerations in the frame $\mathcal{F}_b$;

Then, (10) and (13) are of the form (1) where:

- $x_1 = \rho, x_2 = \dot{\rho}$, $x_k \in \mathbb{R}^3, k = 1, 2$ in the case of the model (10),
- $x_1 = \Theta, x_2 = \varpi$, $x_k \in \mathbb{R}^3, k = 1, 2$ in the case of the model (13).

Furthermore, since the LIDAR provides the measurement of the states $x_1 = \rho$ and $x_2 = \dot{\rho}$ in the case of the model (10), the Star Tracker provides the measurement of the state $x_1 = \Theta$ and the IMU provides the measurement of the state $x_2 = \varpi$ in the case of the model (13), then the problem's formulation obeys to the one stated in section 2 with $C_1 = \mathbb{I}_3$ (see equation (1)). Thus, two separate controllers will be designed, one based on the model (10) for relative position tracking and another one based on the model (13) for attitude tracking.

Following theorem 1, three matrices have to be chosen for each control law, namely $\alpha = diag(\alpha_j)$, $j = \overline{1,3}$, L_1 and L_2. With respect to L_1 and L_2, no real guidelines have been provided in (Zenteno-Torres et al., 2018) for a systemic tuning. However, the reasoning presented in (Zenteno-Torres et al., 2018) is thought valuable, i.e.:

- the SMC law basically results in an inner loop that computes ϕ and an outer loop that computes u,
- $L_i, i = 1, 2$ are error gains (i.e. the terms $L_1 e_y$ and $L_2 \phi$ in equations (3) and (2) respectively) that enters linearly in equations (3) and (2),

Thus, it is reasonable to choose L_1 and L_2 so that $|\lambda_i(L_1)| > |\lambda_i(L_2)|$ meaning that the inner loop is faster than the outer loop. Here, λ_i stands for the eigenvalues of the associated matrix. This boils down to $L_1 = -\mathbb{I}_3$, $L_2 = -0.1\mathbb{I}_3$ for both the attitude loop and relative position loop.
Dealing with the sliding gain diagonal terms α_j, they must be chosen so that they enforce the sliding motion under assumption A.1. For that purpose, it is required to fix (not too conservatively) the terms v_j^+, $j = \overline{1,3}$ for both the attitude and relative position loops. Fundamentally, they represent upper-bounds of the disturbances given by $J^{-1}T_v^b$ (for the case of the attitude control loop) and γ_v^l (for the case of the relative position control loop). These parameters have been estimated using the functional engineering simulator, through a numerous of simulations. This leads to $\alpha = 0.25\mathbb{I}_3$ for the attitude loop and $\alpha = 0.005\mathbb{I}_3$ for the relative position loop.

DOI: 10.13009/EUCASS2019-269

3.4 Simulation results

The performance of the designed SMC control laws are finally assessed using the functional engineering simulator (see figure 1 for an illustration of the played scenario).

A control allocation algorithm is considered to compute the thruster opening commands $u_T(t)$, i.e. to allocate the forces $F_u^b(t)$ and the moments $T_u(t)$ on the thrusters. For this purpose, the control allocation algorithm presented in (Fonod et al., 2015) is retained. It is mainly based on the computation of the optimal generalized inverse of the thruster configuration matrix, in the $\mathcal{L}_2$ sense, i.e. it solves the following optimisation problem:

$$u_T = \underset{u_T \in \mathcal{U}_T = \{u_{T_k} : 0 \leq u_{T_k} \leq \overline{u}_{T_k}\}, k=\overline{1,12}}{argmin} \|W_v(\mathbf{M}u_T - v_r)\|_2 \tag{14}$$

$v_r = [F_u^{b^T} \; T_u^T]^T$ is the vector of the desired force and torque commands, $\overline{u}_{Tk}$ is the maximum opening value of the kth thruster and $\mathbf{M}$ refers to the thruster configuration matrix, see Fig. 2 for an illustration of the position and direction spanned by $\mathbf{M}$. The nonsingular weighting matrix W_v affects the prioritization among force/torque components. The choice of the $\mathcal{L}_2$ norm in (14) results in minimum power allocation.

A path planning (guidance) algorithm is implemented too. It is in charge of generating the position/velocity and attitude/angular velocity profiles for the target acquisition, rendezvous and capture phases. Here, it is based on a spline-based approach to generate smooth profiles in order to approach the target along its velocity axis smoothly. We recall that the simulator considers the nonlinear models and their coupling effects, the second-order zonal harmonic J_2, atmospheric drag, gravity gradient, magnetic disturbances, propellant sloshing and the flexible modes of the solar array.

We recall too that the navigation unit is assumed to be perfect, which is equivalent to say that there is no measurement noise. The investigated scenario used the following parameters:
- Chaser's mass m = 300kg
- Chaser's inertia J = [30 1 1; 1 40 1; 1 1 25]
- Thruster's saturation= 4N, Minimum Impulse Bit = 0.1
- Thruster configuration and geometry of the chaser (including the location of its CoM) as shown in figure 2.
- Sampling time= 0.25s

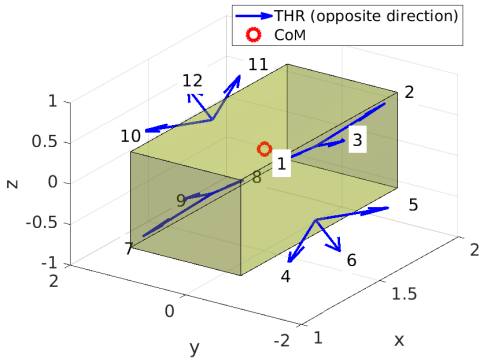

Figure 2: Thruster configuration and geometry of the chaser (including the location of its CoM)

The control signals provided by the attitude and translational sliding-mode controllers are shown in Fig. 3 (top and middle). Fig. 3 top illustrates the time behaviour of the moments $T_u(t)$, whereas Fig. 3 middle illustrates the time behavior of the forces $F_u^{(l)}(t)$. Fig. 3 bottom illustrates the thruster opening commands $u_T(t)$ applied to the set of the 12 thrusters. A zoom is provided for each signal to better appreciate their time behaviour.

Fig. 4 illustrates the behaviour of the attitude $\Theta(t) = [\phi(t) \; \theta(t) \; \psi(t)]^T$ and the relative position $\rho(t) = [\eta(t) \; \zeta(t) \; \xi(t)]^T$. Their references generated by the path planning algorithm (i.e. the guidance unit) are superposed to appreciate the performance of the proposed control strategy. The angular velocity $\varpi(t) = [p(t) \; q(t) \; r(t)]^T$ and the relative velocity $\dot{\rho}(t) = [\dot{\eta}(t) \; \dot{\zeta}(t) \; \dot{\xi}(t)]^T$ is too superposed on the plots. Furthermore, the "target acquisition phase" and the "rendezvous phase" are highlighted for a better understanding of the motion performed by the chaser. We recall that the "target acquisition phase" consists in tracking an attitude reference whereas the "rendezvous phase" consists of a forced translation to the target while maintaining the chaser's attitude to zero so that the capture mechanism is aligned with the

DOI: 10.13009/EUCASS2019-269

target.

It can be inferred from all the presented figures that the obtained results are promising since, as it can be seen, the presented plots exhibit satisfactory tracking performance, i.e. the relative position and the attitude follows their references without saturation of the thrusters (the maximum magnitude reached by the thrusters is close to $2.2N < 4N$). This is confirmed by figure 5 that illustrates the tracking errors.

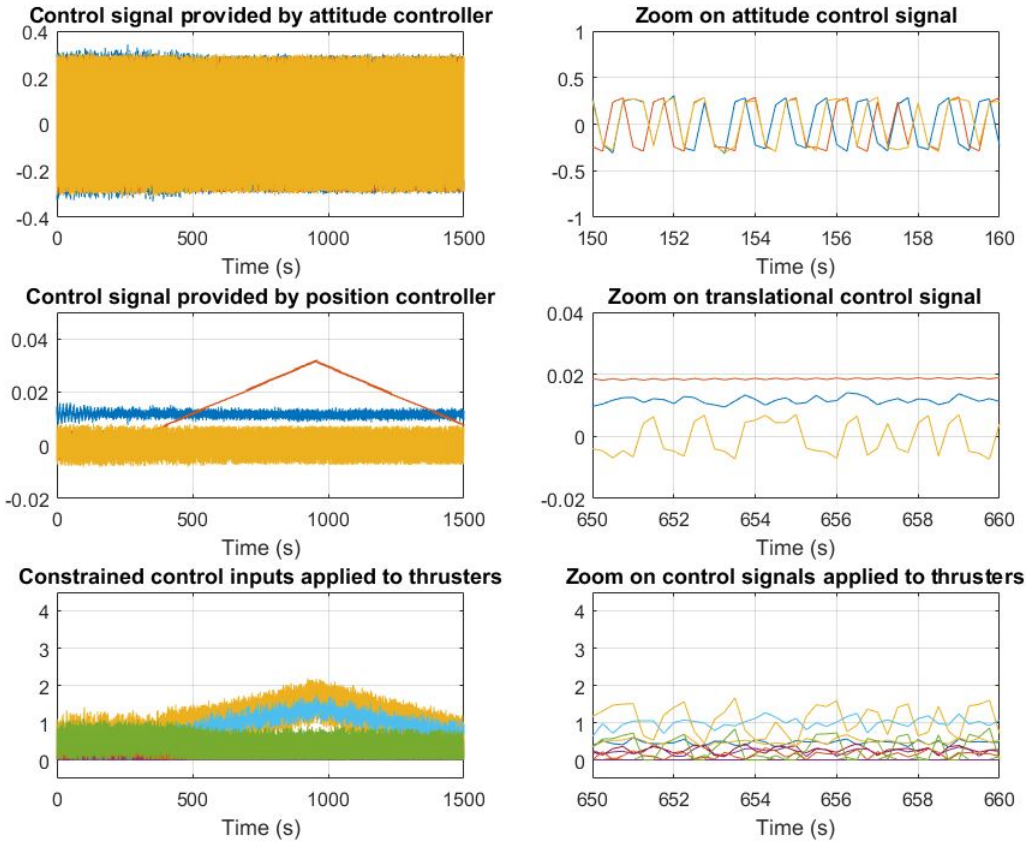

Figure 3: Behaviour of the moments $T_u(t)$ (top), forces $F_u^{(l)}(t)$ (middle) and the thruster opening commands $u_T(t)$ (bottom).

4. Concluding remarks

This paper investigates Sliding Mode Control (SMC) techniques for rendezvous missions in space. The proposed control architecture is based on a SMC used in a backstepping setup. The proposed methodology is applied to a functional engineering simulator that accurately simulates a rendezvous mission between a chaser spacecraft and a passive target onto a circular orbit around Earth, taking into account the coupling between attitude and translational motions, propellant sloshing, modes of the flexible appendages and the most dimensioning space disturbances (e.g. second zonal harmonic J_2, atmospheric drag, magnetic disturbance). Simulation results demonstrate the potential of the proposed approach.

Acknowledgement

The authors gratefully acknowledge the financial support from CONACyT under grant 440473 (CVU 594664) and the financial support by SIP-IPN under grant 20180865 and to the CDA-IPN.

DOI: 10.13009/EUCASS2019-269

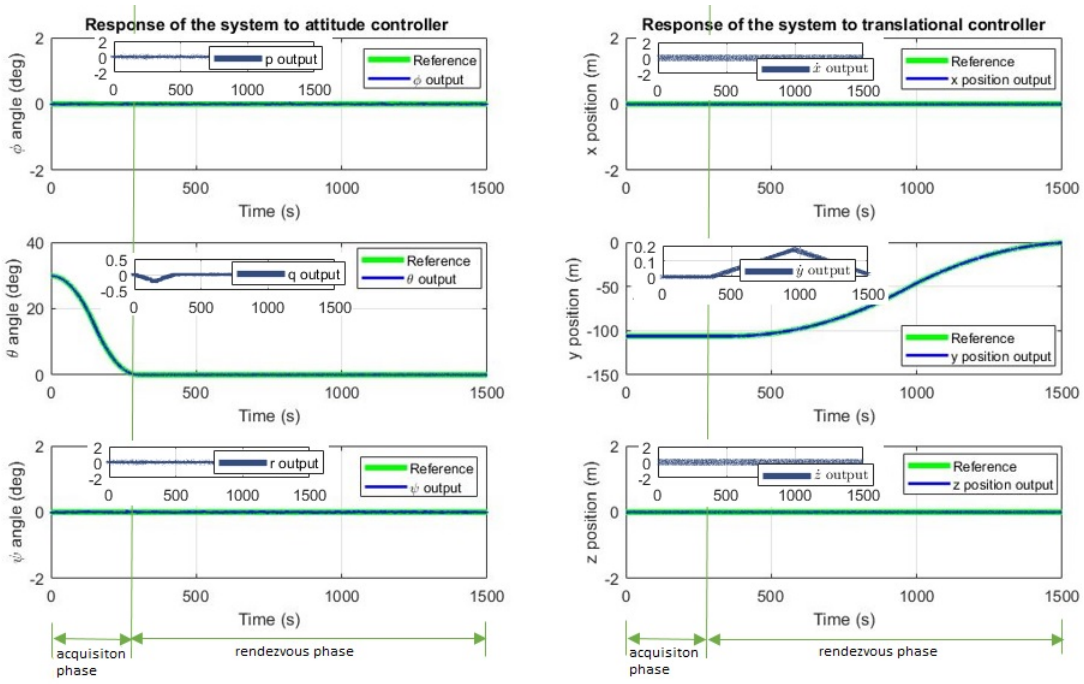

Figure 4: Behaviour of the attitude $\Theta(t) = [\phi(t)\ \theta(t)\ \psi(t)]^T$ (left), the relative position $\rho(t) = [\eta(t)\ \zeta(t)\ \xi(t)]^T$ (right) and their references.

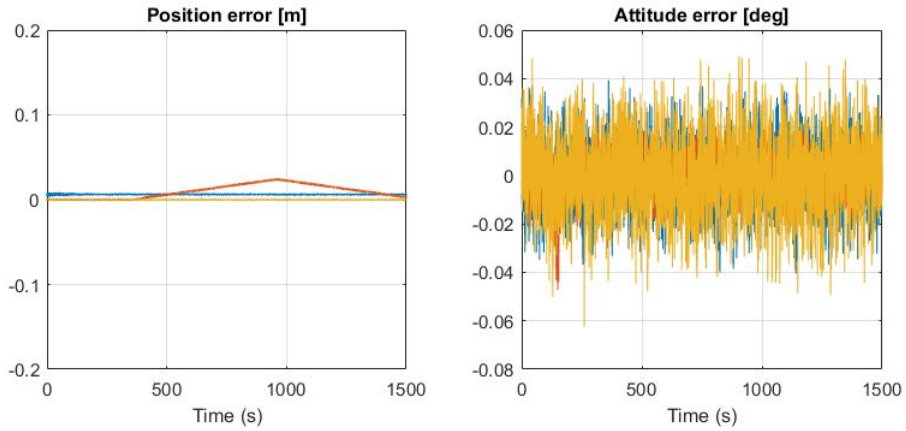

Figure 5: Tracking errors: relative position (left), attitude (right).

References

Colmenarejo, P., Branco, J., Santos, N., Arroz, P., Telaar, J., Strauch, H., Ott, C., Reiner, M., Henry, D., Jaworski, J., Papadopoulos, E., Visentin, G., Ankersen, F., and Gil-Fernandez, J. (2018a). Methods and outcomes of the COMRADE project - design of robust coupled control for robotic spacecraft in servicing missions: trade-off between hinf and nonlinear lyapunov-based approaches. In *International Astronautical Congress 2018*, October. Bremen, Germany.

Colmenarejo, P., Briz, J., Alcalde, A., Peters, T., Dubanchet, V., Henry, D., Menon, P., and Ankersen, F. (2018b). Advanced gnc for in-orbit autonomous assembly of flexible vehicles âĂŞ ioa-gnc. In *International Astronautical Congress 2018*, October. Bremen, Germany.

Colmenarejo, P., Telaar, J., Ott, C., Branco, J., Jarowski, J., Papadopoulos, E., Henry, D., and Visentin, G. (2017). COMRADE: Control and management of robotics active debris removal. In *Clean Space Industrial days*, 24–27 October. ESA, Netherlands.

DOI: 10.13009/EUCASS2019-269

Cong, B., Liu, X., and Chen, Z. (2013). Backstepping based adaptive sliding mode control for spacecraft attitude maneuvers. *Aerospace Science and Technology*, 30(1), 1–7.

Crassidis, J.L. and Markley, F.L. (1996). Sliding mode control using modified rodrigues parameters. *Journal of Guidance, Control, and Dynamics*, 19(6), 1381–1383.

Davila, J.A. and Gómez-Cortes, G.C. (2013). Attitude control of spacecraft using robust backstepping controller based on high order sliding modes. In *AIAA Guidance, Navigation, and Control (GNC) Conference*, 5121.

De Loza, A.F., Cieslak, J., Henry, D., Zolghadri, A., and Fridman, L.M. (2015). Output tracking of systems subjected to perturbations and a class of actuator faults based on hosm observation and identification. *Automatica*, 59, 200–205.

Dong, J., Li, C., Jiang, B., and Sun, Y. (2017). Fixed-time nonsingular terminal sliding mode control for spacecraft rendezvous. In *Control And Decision Conference (CCDC), 2017 29th Chinese*, 5340–5345. IEEE.

Ebrahimi, B., Bahrami, M., and Roshanian, J. (2008). Optimal sliding-mode guidance with terminal velocity constraint for fixed-interval propulsive maneuvers. *Acta Astronautica*, 62(10-11), 556–562.

Fonod, R., Henry, D., Charbonnel, C., Bornschlegl, E., Losa, D., and Bennani, S. (2015). Robust fdi for fault-tolerant thrust allocation with application to spacecraft rendezvous. *Control Engineering Practice*, 42, 12–27.

Gao, X., Teo, K.L., and Duan, G.R. (2012). Non-fragile robust H_∞ control for uncertain spacecraft rendezvous system with pole and input constraints. *International Journal of Control*, 85(7), 933–941.

Henry, D., Cieslak, J., Zenteno-Torres, J., Colmenarejo, P., Branco, J., Santos, N., Serra, P., Telaard, J., Strauch, H., Giordano, A., Stefano, M., Ott, C., Reiner, M., Jaworski, J., Papadopoulos, E., Visentin, G., Ankersen, F., and Gil-Fernandez, J. (2019). Model-based fault diagnosis and tolerant control: the ESAâĂŹs e.Deorbit mission. In *European Control Conference - ECC'2019*, 25–28 June. Naples, Italy.

Hu, Q., Cao, J., and Zhang, Y. (2009). Robust backstepping sliding mode attitude tracking and vibration damping of flexible spacecraft with actuator dynamics. *Journal of Aerospace Engineering*, 22(2), 139–152.

Huang, Y. and Jia, Y. (2017). Robust adaptive fixed-time 6 dof tracking control for spacecraft non-cooperative rendezvous. In *Control Conference (CCC), 2017 36th Chinese*, 3153–3158. IEEE.

Imani, A. and Beigzadeh, B. (2016). Robust control of spacecraft rendezvous on elliptical orbits: Optimal sliding mode and backstepping sliding mode approaches. *Proceedings of the Institution of Mechanical Engineers, Part G: Journal of Aerospace Engineering*, 230(10), 1975–1989.

Krogstad, T.R., Kristiansen, R., Gravdahl, J.T., and Nicklasson, P.J. (2007). Pid+ backstepping control of relative spacecraft attitude. *IFAC Proceedings Volumes*, 40(12), 928–933.

Krstic, M. and Tsiotras, P. (1999). Inverse optimal stabilization of a rigid spacecraft. *IEEE Transactions on Automatic Control*, 44(5), 1042–1049.

Levant, A. (2003). Higher-order sliding modes, differentiation and output-feedback control. *International journal of Control*, 76(9-10), 924–941.

Liu, H., Shi, X., Bi, X., and Zhang, J. (2016). Backstepping-based terminal sliding mode control for rendezvous and docking with a tumbling spacecraft. *International Journal of Innovative Computing, Information and Control*, 12(3), 929–940.

Lo, S.C. and Chen, Y.P. (1995). Smooth sliding-mode control for spacecraft attitude tracking maneuvers. *Journal of Guidance, Control, and Dynamics*, 18(6), 1345–1349.

Mboup, M., Join, C., and Fliess, M. (2007). A revised look at numerical differentiation with an application to nonlinear feedback control. In *Control & Automation, 2007. MED'07. Mediterranean Conference on*, 1–6. IEEE.

Montenbruck, O. and Gill, E. (2012). *Satellite Orbits. Models, Methods, Applications (4th Ed.)*. Springer.

Park, J.U., Choi, K.H., and Lee, S. (1999). Orbital rendezvous using two-step sliding mode control. *Aerospace science and technology*, 3(4), 239–245.

Preda, V., Cieslak, J., Henry, D., Bennani, S., and Falcoz, A. (2017). A H_infty/mu solution for microvibration mitigation in satellites: A case study. *Journal of Sound and Vibrations*, 399, 21–44. doi:10.1016/j.jsv.2017.03.015.

DOI: 10.13009/EUCASS2019-269

Preda, V., Cieslak, J., Henry, D., Bennani, S., and Falcoz, A. (2018). Robust microvibration mitigation and pointing performance analysis for high stability spacecraft. *International Journal of Robust and Nonlinear Control*, 28(18), 5688 – 5716. doi:10.1002/rnc.4338.

Shtessel, Y., Edwards, C., Fridman, L., and Levant, A. (2014). *Sliding mode control and observation*, volume 10. Springer.

Tournes, C., Shtessel, Y., and Foreman, D. (2011). Automatic space rendezvous and docking using second order sliding mode control. In *Sliding Mode Control*. InTech.

Wang, Q., Zhou, B., and Duan, G.R. (2015). Robust gain scheduled control of spacecraft rendezvous system subject to input saturation. *Aerospace Science and Technology*, 42, 442–450.

Wied, B. (1998). *Space vehicle dynamics and control*. Reston, VA: American Institute of Aeronautics and Astronautics.

Zenteno-Torres, J., Cieslak, J., Henry, D., and Davila, J. (2018). A tracking backstepping sliding-mode control for spacecraft rendezvous with a passive target. In *2018 UKACC 12th International Conference on Control*, 5–7 September. Sheffield, UK. doi:10.1109/CONTROL.2018.8516895.

Zenteno-Torres, J., Cieslak, J., Henry, D., and Davila, J. (2019). A super-twisting sliding mode control in a backstepping setup for rendezvous with a passive target. In *21st IFAC Symposium on Automatic Control in Aerospace - ACA 2019*, 27–30 August. Cranfiled campus, UK.

Zhao, L., Jia, Y., and Matsuno, F. (2013). Adaptive time-varying sliding mode control for autonomous spacecraft rendezvous. In *Decision and Control (CDC), 2013 IEEE 52nd Annual Conference on*, 5504–5509. IEEE.